J. Electrochem. Sci. Eng. **15(3)** (2025) 2589; http://dx.doi.org/10.5599/jese.2589

Open Access : : ISSN 1847-9286
https://pub.iapchem.org/ojs/index.php/JESE

Original scientific paper

Immobilized triton X-100 voltammetric sensor for the simultaneous detection of sunset yellow and tartrazine

Puneeth[1], B. E. Kumara Swamy[1,✉] and S. C. Sharma[2]

[1]*Departmen of PG Studies and Research in Industrial Chemistry, Kuvempu University, Jnana Sahyadri Shankaraghatta, Shimoga Dist, Karnataka 577451, India*
[2]*Jain University, Bangalore, Karnataka, 560 069, India*

Corresponding author: ✉kumaraswamy21@yahoo.com

Received: December 5, 2024; Accepted: February 26, 2025; Published: April 1, 2025

Abstract

In this study, we developed a sensor utilizing a pencil graphite electrode combined with triton X-100 surfactant prepared by immobilization technique. This modified electrode can concurrently detect sunset yellow (SY) and tartrazine (TZ) in a binary mixture. Both compounds are synthetic azo dyes known to have hazardous effects on human health, including the potential for malignant growth at prolonged exposure. The modified electrode shows remarkable sensitivity toward SY and TZ individually and in combination. We conducted pH studies, scan rate analysis, reproducibility tests, and simultaneous detection studies using cyclic voltammetry. Differential pulse voltammetry technique was used to investigate concentration and mutual interference effects. Our pH study found that the maximum anodic peak current for SY occurs at pH 7.4, while TZ shows a higher current at pH 7.0. The scan rate analysis indicated that the anodic reactions of both dyes are controlled by the adsorption process. The limit of detection (LOD) and limit of quantification (LOQ) for SY are 0.17 and 0.59 µM, respectively, while for TZ, the LOD and LOQ are 0.67 and 2.26 µM, respectively. The surfactant-modified pencil electrode demonstrates excellent peak separation between SY and TZ in a binary mixture, exhibiting stability of 86.3 % for sunset yellow and 65 % for tartrazine over 25 cycles.

Keywords

Synthetic azo dyes; binary mixture; modified pencil graphite electrode; non-ionic surfactant; immobilization method

Introduction

Azo dyes are a class of chemicals widely used in various fields, including food [1], leather [2], textile [3], and pharmaceutical industries [4], to impart attractive colours. In the food industry, these dyes enhance both colour and taste. In the leather industry, they are applied to give products appealing colours, increasing their marketability. Pharmaceuticals utilize dyes to differentiate between various drugs by colour. The increasing use of azo dyes is attributed to their low cost and high attractiveness. Depending on the manufacturer, these dyes can be synthesized through natural and synthetic methods [5]. However, their use raises safety concerns because of their toxic nature. Prolonged exposure to these dyes may pose health risks [6]. Nowadays, almost every packaged food product contains artificial colours. In some cases, dyes are used without being listed on labels, and instances of using higher concentrations than those indicated have also been reported [7]. This has heightened interest among researchers in developing methods to detect azo dyes. Azo dye manufacturers focus on cost-effectiveness, stability, solubility, versatility (used in baked goods, snacks, and ice creams), and regulatory approval [8]. As a result, they often use dyes like sunset yellow (SY) and tartrazine (TZ), which meet these criteria.

SY is a synthetic azo dye with various applications, as mentioned earlier. It is commonly used in many food products, including gummies, dairy items, baked goods, ice creams, yogurts, and other locally popular foods. Historically, SY has been analysed using techniques such as high-performance liquid chromatography (HPLC) [9], capillary electrophoresis [10], mass spectrometry [11], and thin-layer chromatography [12]. Tartrazine is another important synthetic azo dye, primarily used in food products such as confectionaries, dairy items, and gummies[13]. This dye is often analysed and validated using HPLC [14], mass spectrometry [15] and capillary electrophoresis [16] as well. In addition to these methods, both SY and TZ can be detected using electrochemical techniques [17], which are cost-effective, less time-consuming, and provide reliable results.

The electrochemical techniques have already been used to develop sensors by employing various carbon-based working electrodes, such as glassy carbon electrodes [18], carbon paste electrodes [19], and graphite pencil electrodes [20]. Glassy carbon and carbon paste electrodes can be modified with nanomaterials [21,22], polymer films [23,24], and surfactants [25,26]. The pencil electrode also uses nanomaterials, polymer films [27], and surfactants for modification [28]. Surfactants, *i.e*. surface-active agents, have extensive use across multiple industries, including food [29], paints [30], and pharmaceuticals [31]. They consist of two components: a hydrophilic head and a hydrophobic tail. Triton X-100 is poly(ethylene glycol) p-nonyl phenyl ether due to its effective emulsifying, wetting, and solubilizing properties, which is suitable for voltammetric detection of SY and TZ. Triton X-100 has previously been employed in various sensor research efforts. The modification of electrodes with this surfactant can be performed using the pretreatment method [32] and immobilization [33] technique.

Although SY and TZ have been detected using various nanomaterials [34], polymer films [35], and carbon-based electrodes, the same opportunity remains for TX-100 as a modifier for graphitic pencil electrodes. In the present work, a pencil graphite electrode was used for the electrochemical detection of SY and TZ by using the immobilization method. The detections were simultaneously validated with a variation of scan rate (*v*), concentration and mutual interference studies at surfactant-modified graphite pencil electrodes, leading to simple electrochemical sensor development. Electrochemical reactions that are substantial for the detection of SY and TZ are presented in Schemes 1 and 2.

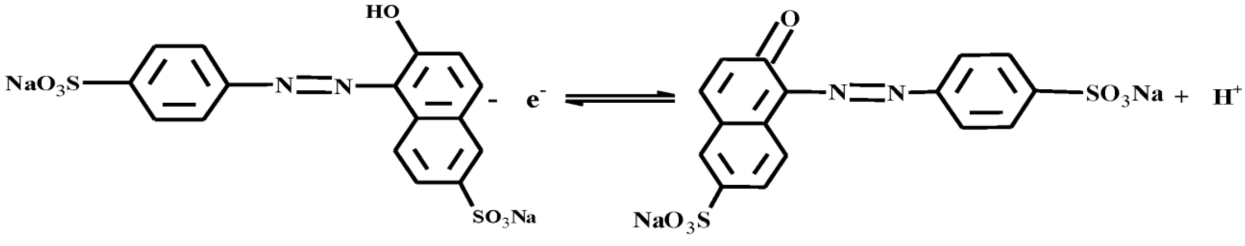

Scheme 1. *Redox scheme of sunset yellow*

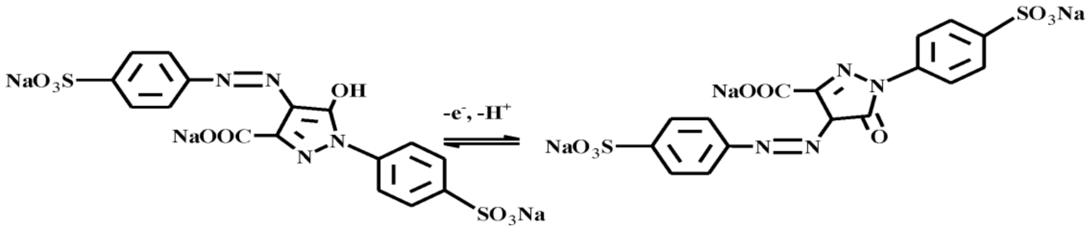

Scheme 2. *Oxidation scheme of tartrazine*

Experimental

Chemicals and apparatus required

Sunset yellow was brought from Sigma Aldrich and tartrazine was procured from Loba chemicals, Triton X-100, Na_2HPO_4, NaH_2PO_4, and KCl were brought from Himedia. The electrochemical studies were carried out using the potentiostat CHI 660c. A graphite pencil electrode was used as a working electrode, a saturated calomel electrode (SCE) was used as a reference electrode, and a platinum wire was used as an auxiliary electrode. All the experiments were carried out at lab temperature.

Preparation of electrodes

The graphite pencil electrode (PE), with a diameter of 0.7 mm, was procured locally and used as the bare electrode. The modified graphite pencil electrode (TX-100/MPE) was prepared using the immobilizing technique, where 1 ml of 20 µM TX-100 was directly added to the analyte solution, and then the PE electrode was dipped into the analyte solution. After regular intervals (0, 15, 30 and 45 s), CVs were recorded to determine the optimized CV (TX-100/MPE).

Results and discussion

Immobilization of TX-100

CVs were taken to select the optimized time needed for the immobilization of TX-100 at PE, which would give the best analyte response. As represented by Figure 1A showing CVs for 1mM SY in 0.2 M PBS, pH 7.4 at TX-100/MPE, there is an increase of anodic peak current (I_{pa}) as immobilization time (t) was increased from 0 to 30 s, while after 45 s, the anodic current is decreased (Figure 1B).

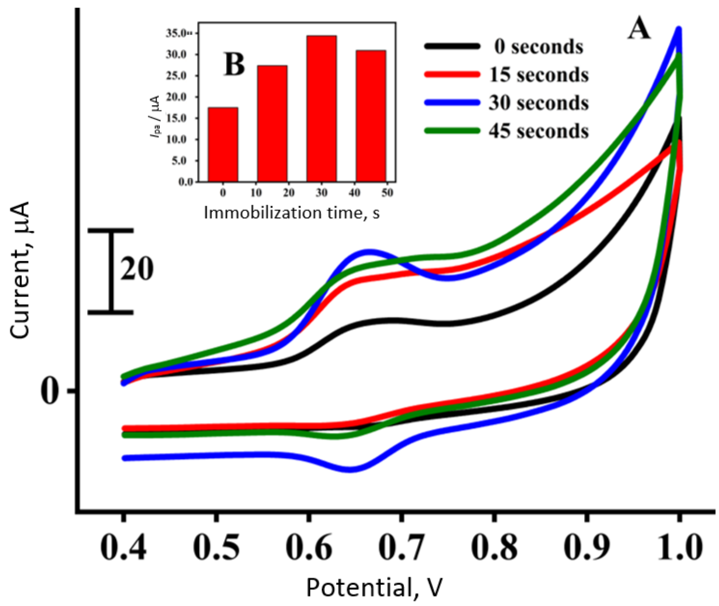

Figure 1. *(A) CVs (v = 100 mV s^{-1}) of 1 mM SY in 0.2 M PBS, pH 7.4 electrolyte solution at TX-100/MPE formed after different immobilization times of TX-100 at PE surface; (B) Graph of* I_{pa} *versus* t

Figure 2A represents the CVs for finding the optimized immobilization time of TX-100 at PE in 0.2 M PBS, pH 7.4, containing 1 mM TZ analyte. The CV shows an increase in peak current till 30 s and then it decreases when the immobilization time reaches 45 seconds (Figure 2B). On the basis of Figures 1B and 2B, all subsequent experiments with SY and TZ were carried out using the same optimized time for TX-100 immobilization at a PE surface of 30 s.

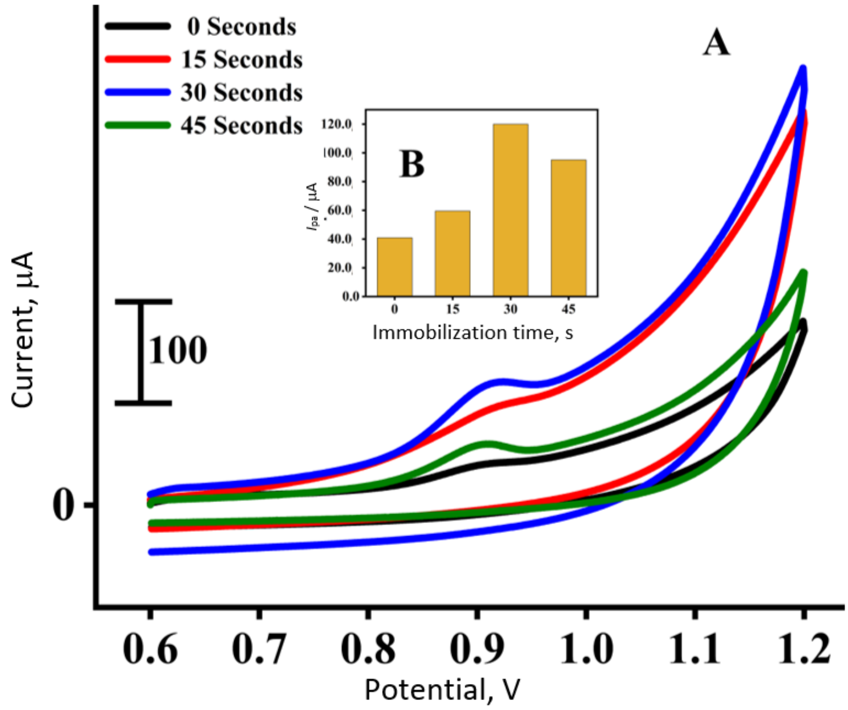

Figure 2. *(A) CVs (ν = 100 mV s^{-1}) of 1 mM TZ in 0.2 M PBS of 7.4 pH electrolyte solution at TX-100/MPE formed after different immobilization times of TX-100 at PE surface; (B) Graph of* I_{pa} *versus* t

SY and TZ responses at TX-100/MPE at different pH

The CV technique was applied to monitor the effects of pH variations (6.2, 6.6, 7.0, 7.4 and 7.8) of supporting electrolyte (0.2 M PBS) on the response of 1 mM SY at TX-100/MPE. Figure 3A shows that as pH increases, the anodic peak potential (E_{pa}) shift occurs from a higher to a lower value, which is validated by the Epa versus pH curve in Figure 3B. The graph shows the linear decrease of E_{pa} as the pH increases, where the slope is -64 mV, which is almost equal to the Nernstian value of -59 mV, indicating that protons and electrons are shared in a 1:1 ratio (Scheme 1). The linear regression equation is defined as E_{pa} = 1.16085 - 0.06475 pH and the R^2 value was found to be 0.998. The anodic peak current (I_{pa}) *vs.*pH is represented in Figure 3C, showing a rise in I_{pa} as pH increases from 6.2 to 7.4, while at pH 7.8, the current decreases [36,37].

Figure 4A represents the effects of the pH variation of 0.2 M PBS containing 1 mM TZ at TX/100MPE recorded *via* the CV technique. As the pH increases, E_{pa} decreases to a negative value, which is represented in Figure 4B. The slope of the curve was found to be -53 mV, which is near the theoretical value of -59 mV and represents that electrons and protons are equally shared in the oxidation process (Scheme 2). The linear regression equation was defined as E_{pa} =1.192 - 0.053 pH (R^2=0.998). The I_{pa} versus pH graph is shown in Figure 4C, representing a rise in anodic peak current as pH increases from 6.2 to 7.0 and then a decrease for subsequent pH increase**s**. According to the results obtained in Figures 3C and 4C, the remaining studies for both synthetic azo dyes were carried out using a physiological pH of 7.4 [38,39].

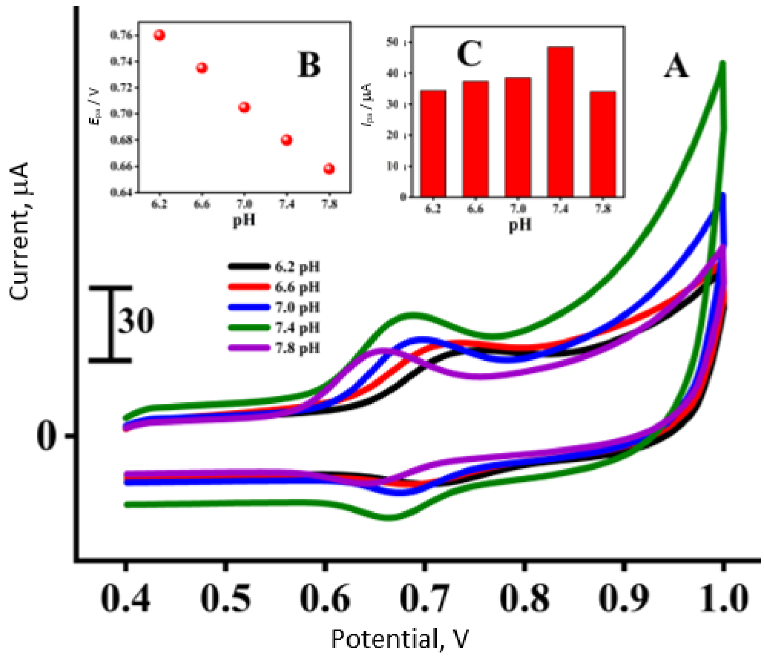

Figure 3. *(A) CVs for 1 mM SY in 0.2 M PBS of varying pH at TX-100/MPE; (B)* E_{pa} vs. *pH; (C)* I_{pa} vs. *pH*

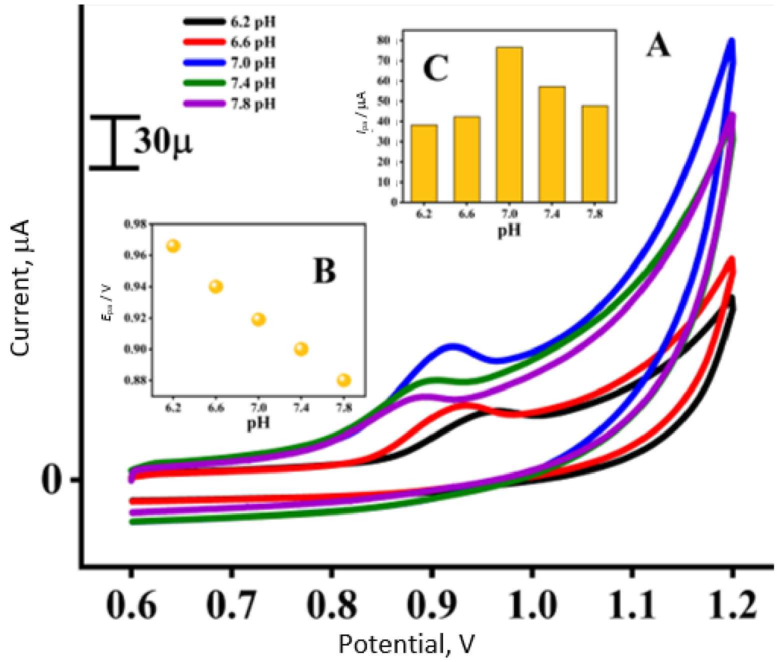

Figure 4. *(A) CVs for 1 mM TZ in 0.2 M PBS of varying pH at TX-100/MPE; (B)* E_{pa} vs. *pH; (C)* I_{pa} vs. *pH*

Comparison of SY and TZ responses at BPE and TX-100/MPE

Figure 5 represents the CVs for 1 mM SY in 0.2 M PBS, pH 7.4, at a scan rate of 100 mV s^{-1}. The black dotted line represents the CV of SY at the bare graphite pencil electrode (BPE) and the red solid line represents the CV of SY at TX-100/MPE. The I_{pa} of SY at TX-100/MPE is 34.53 µA, while the I_{pa} for SY at BPE is 3.647 µA, comparing the current values shows nearly 10 folds higher anodic peak current of SY at TX-100/MPE than BPE [40,41].

The CVs of 1 mM TZ at the scan rate 100 mV s^{-1} in 0.2 M PBS of 7.4 pH are represented in Figure 6. The black dotted line represents the CV of TZ at BPE and the solid yellow line represents the CV of TZ at TX-100/MPE. The I_{pa} of TX-100/MCPE is 10 times higher compared to the I_{pa} of BPE. From these results (Figures 5 and 6), it can be concluded that the increase in current in CVs of both dyes is due to the surface activity of TX-100 surfactant [42].

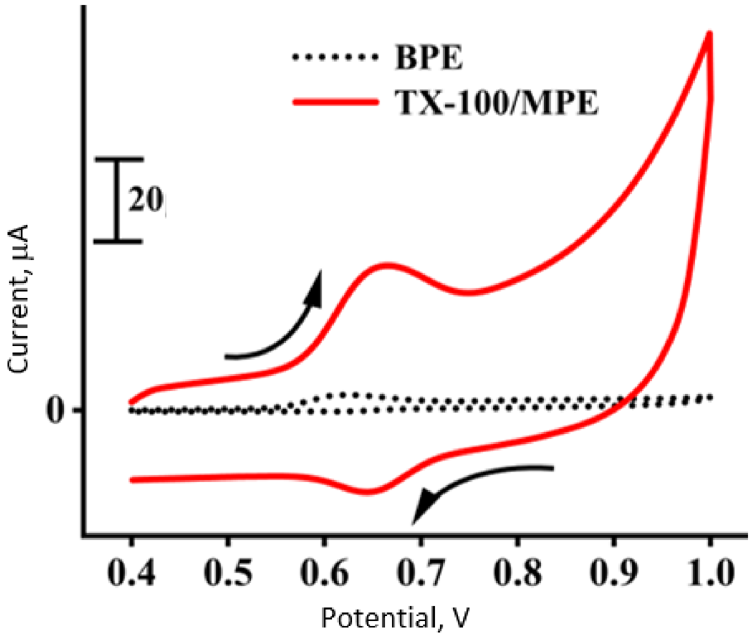

Figure 5. *CVs (v = 100 mV s^{-1}) of 1 mM SY in 0.2 M PBS, pH 7.4, at TX-100/MPE (red solid line) and BPE (black dotted line)*

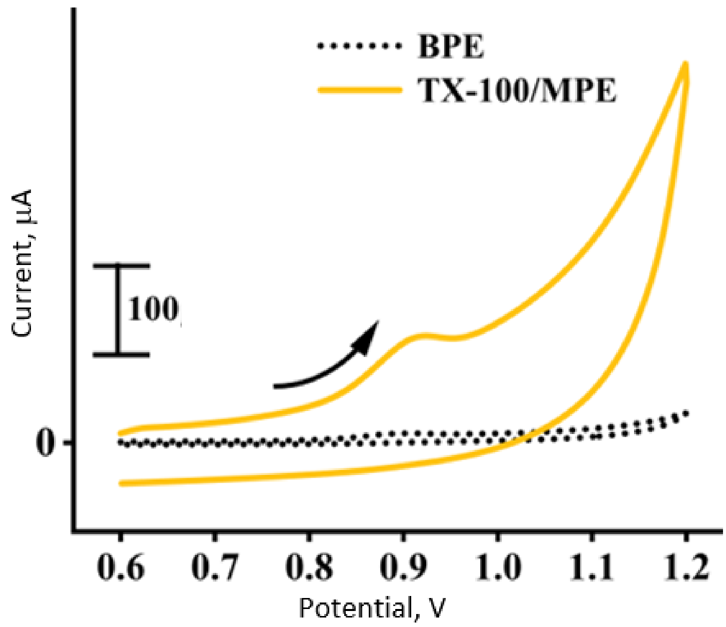

Figure 6. *CVs (v = 100 mV s^{-1}) of 1 mM TZ in 0.2 M PBS, pH 7.4, at TX-100/MPE (yellow solid line) and BPE (black dotted line)*

Scan rate effects on anodic peak currents of SY and TZ

The resultant CVs, recorded at different sweep rates (50 to 500 mV s^{-1}) at TX-100/MPE for 1 mM SY in 0.2 M PBS, pH 7.4, are represented in Figure 7A. The anodic peak current increases subsequently with the increase in scan rate and has a slight shift in anodic potential. The graph of I_{pa} *vs.* scan rate is represented in Figure 7B, and linear regression for the straight line is defined as: I_{pa} = 2.18 ×10^{-4} (v) + 5.596 ×10^{-6} (R^2 = 0.997). Figure 7C shows the graph of log I_{pa} versus log v, with a slope of 0.706, indicating that the process involved is controlled by adsorption.

Figure 8A presents CVs measured under the variation of scan rate for 1 mM TZ in 0.2 M PBS of 7.4 at TX-100/MPE. As the sweep rate increases, the resultant anodic peak current increases with a slight shift in peak potential.

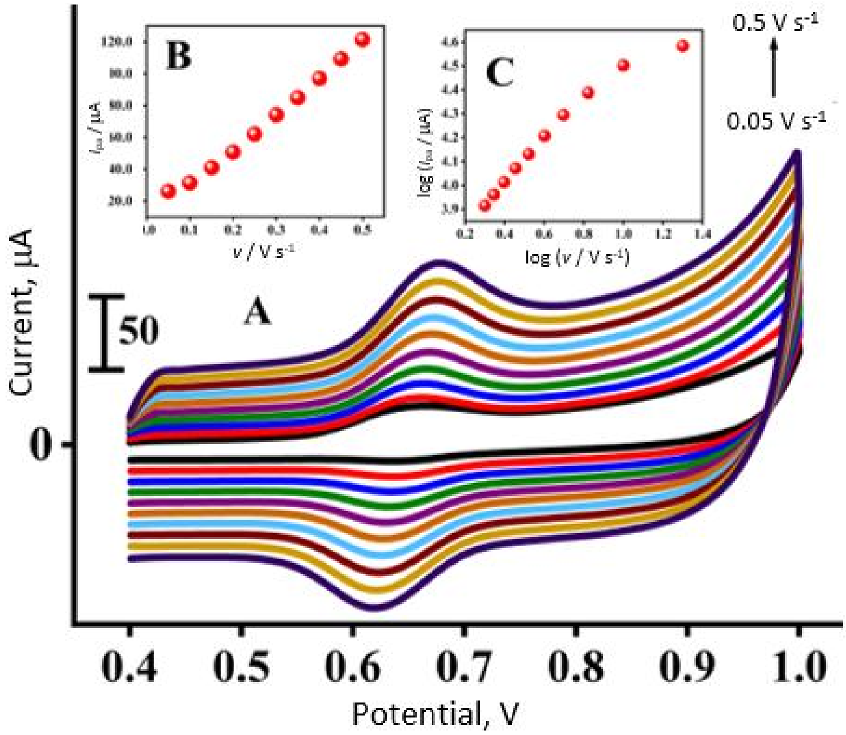

Figure 7. *(A) CVs at different sweep rates for 1 mM SY in 0.2 M PBS, pH 7.4, at TX-100/MPE; (B)* I_{pa} vs. ν*; (C) log* I_{pa} vs. *log* ν

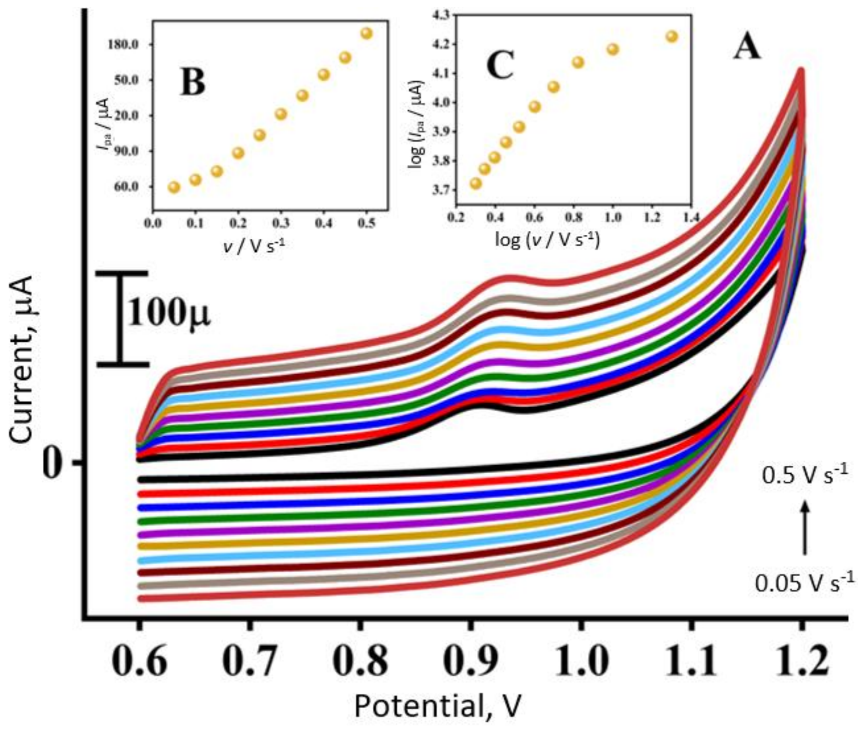

Figure 8. *(A) CVs at different sweep rates for 1 mM TZ in 0.2 M PBS, pH 7.4, at TX-100/MPE; (B)* I_{pa} vs. ν*; (C) log* I_{pa} vs. *log* ν

The graph of I_{pa} *versus* scan rate is represented in Figure 8B, where the resulting linear regression equation is: I_{pa} = 2.986×10^{-4} v + 3.392×10^{-5} (R^2 = 0.993). The log I_{pa} versus log v graph is shown in Figure 8C, which indicates a slope of 0.533, suggesting that the electrode shows an adsorption-controlled phenomenon [43].

Effect of concentration of SY and TZ at TX-100/MPE

The differential pulse voltammetric (DPV) technique was used to detect the concentration effects of SY and TZ at TX-100/MPE using 0.2 M PBS, pH 7.4 solution. Figure 9A represents the concentration effect of SY (1 to 6 µM) at TX-100/MPE. It is seen that as the concentration of SY increases, the subsequent anodic peak current also increases. This trend was further proven by Figure 9B, which shows that the increase in peak current is linear and the linear regression equation is defined as: $I_{pa} = 1.44\times10^{-5}\, C_{SY} + 4.746\times10^{-5}$ ($R^2 = 0.999$).

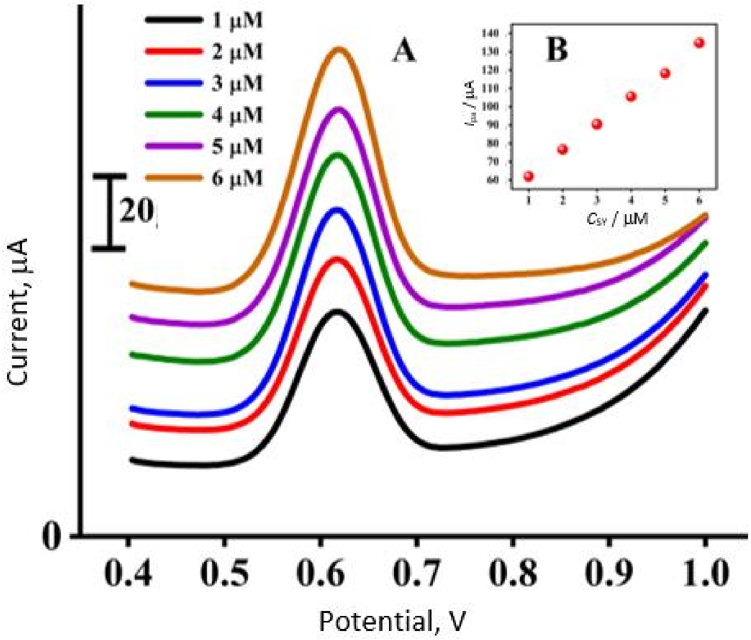

***Figure 9.** (A) DPVs for rising concentrations of SY in 0.2 M PBS, pH 7.4 at TX-100/MPE; (B)* I_{pa} vs. *concentration of SY*

Figure 10A demonstrates the effect of the concentration of TZ (1 to 8 µM) at TX-100/MPE. When the concentration increases the peak current also increases simultaneously, this was further proven by Figure 10(B), where linear regression is defined as: $I_{pa} = 6.303\times10^{-6}\, C_{TZ} + 1.103\times10^{-5}$ ($R^2 = 0.996$).

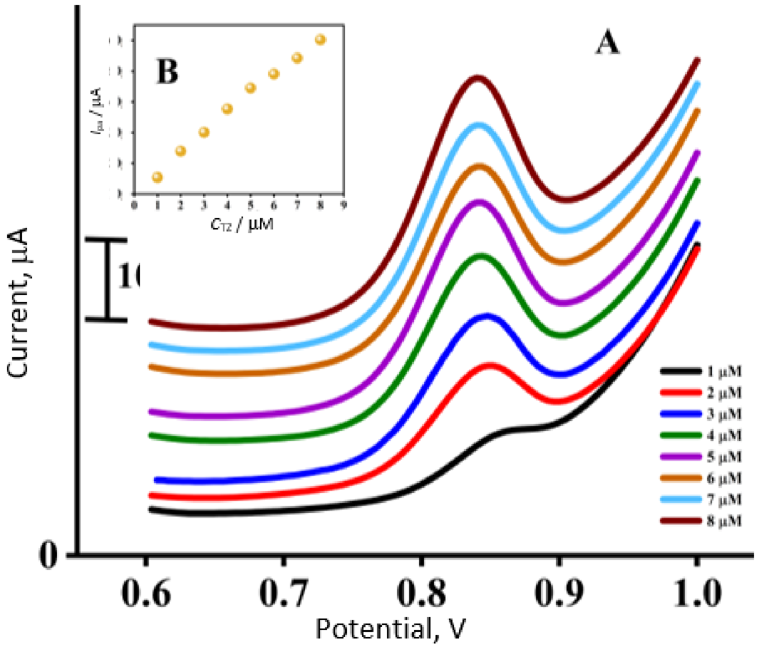

***Figure 10.** (A) DPV for rising concentrations of TZ in 0.2 PBS, pH 7.4 at TX-100/MPE; (B)* I_{pa} vs. *concentration of TZ*

Equations (2) and (3) were used to calculate the limit of detection (LOD) and limit of quantification (LOQ):

$$\text{LOD} = 3S/M \tag{2}$$

$$\text{LOD} = 10S/M \tag{3}$$

Here, S is the standard deviation, and M is the slope of a straight line. The LOD and LOQ of SY at TX-100/MPE were found to be 0.17 and 0.59 µM, respectively. TZ at TX-100/MPE has a LOD of 0.67 µM and LOQ of 2.26 µM. Some reported literature data on LOD values already obtained by voltammetric determination of SY and TZ at different electrodes are presented in Tables 1 and 2.

***Table 1**. LOD values of TZ for some reported electrodes*

Electrode	Method	LOD, µM	Reference
PGMCPE	CV	2.045	[44]
CNF/AuNP-CPE	DPV	2.64	[45]
SDSMCPE	CV	5.2	[46]
Gr/PLPA/PGE	DPV	1.54	[47]
TX-100/MPE	DPV	0.67	Present work

***Table 2.** LOD values of SY for some reported electrodes*

Electrode	Method	LOD, µM	Reference
ePad	CV	2.38	[48]
PTA/GCE	DPV	0.5	[49]
Chitosan/graphene	CV	0.6	[50]
GC/EGr-1	LSV	1.8	[51]
TX-100/MPE	DPV	0.17	Present work

Reproducibility of TX-100/MPE

The CV technique was employed to evaluate the stability of TX-100/MPE for SY and TZ in 0.2 M PBS at pH 7.4. Figure 11 presents CVs of 1 mM SY at TX-100/MPE over 25 cycles, while Figure 12 displays CVs for 1 mM TZ at TX-100/MPE. Stability was determined using the formula I_{pn}/I_{p1} [52], where I_{pn} represents the peak current of the 25th cycle and I_{p1} denotes the peak current of the 1st cycle. The stability of TX-100/MPE was found to be 86.3 % for SY and 65 % for TZ, respectively [53].

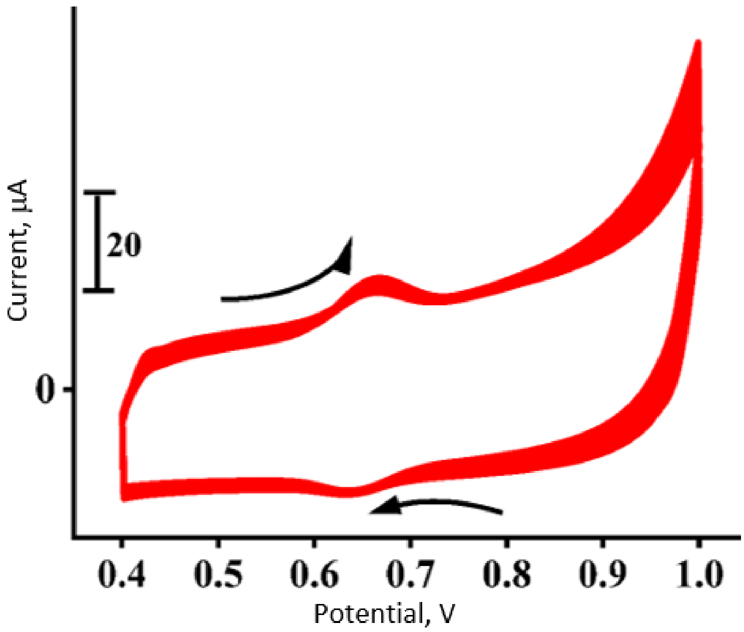

***Figure 11.** CVs (v = 100 mVs^{-1}) for 1 mM SY in 0.2 M PBS, pH 7.4 at TX-100/MPE for 25 cycles*

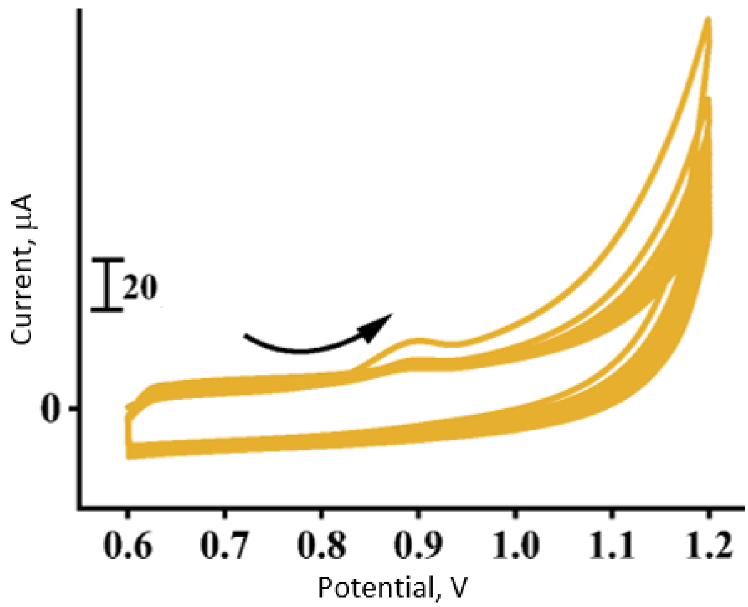

Figure 12. *CVs (v = 100 mVs^{-1}) for 1 mM TZ in 0.2 M PBS, pH 7.4, at TX-100/MPE for 25 cycles*

Simultaneous responses of SY and TZ at TX-100/MCP and BPE

Figure 13 displays the CV of 1 mM SY and 1 mM TZ in a binary mixture at TX-100/MPE in 0.2 M PBS, pH 7.4. The black dotted line represents the CVs for SY and TZ mixture at BPE, showing a current peak for SY at an anodic peak potential of 0.675 V and a current peak for TZ at 0.897 V. The green solid line represents the CVs for both SY and TZ at TX-100/MPE, indicating a shift in potential compared to BPE; the anodic peak potential for SY appears at 0.682 V, while TZ shows a peak potential at 0.937 V. Additionally, the peak currents at TX-100/MPE for both SY and TZ increase nearly three times compared to BPE. This demonstrates that TX-100/MPE can detect SY and TZ in a binary mixture [54].

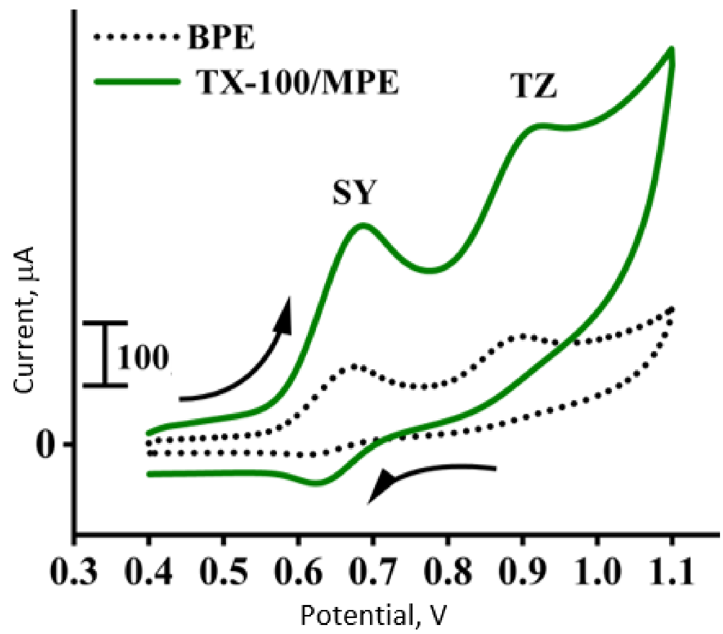

Figure 13. *Comparative CVs of 1 mM SY and 1 mM TZ binary mixture in 0.2 M PBS, pH 7.4 at BPE (black dotted line) and TX-100/MPE (green solid line)*

Selectivity study of SY and TZ at TX-100/MPE

The differential pulse voltammetry (DPV) method was utilized to investigate the selectivity of SY in the presence of TZ, and *vice versa*, at TX-100/MPE in 0.2 M PBS, pH 7.4. Figure 14A illustrates the selectivity of SY when TZ is maintained at a constant concentration of 1 mM. As the concentration of SY increases from 1 to 5 mM, the anodic peak current of SY rises significantly, while the peak current of TZ shows only a negligible increase. Figure 14B confirms that this increase in the peak current of SY is linear, described by the equation I_{pa} = 8.745×10^{-6} C_{SY} + 4.859×10^{-6} (R^2=0.996) [55-57].

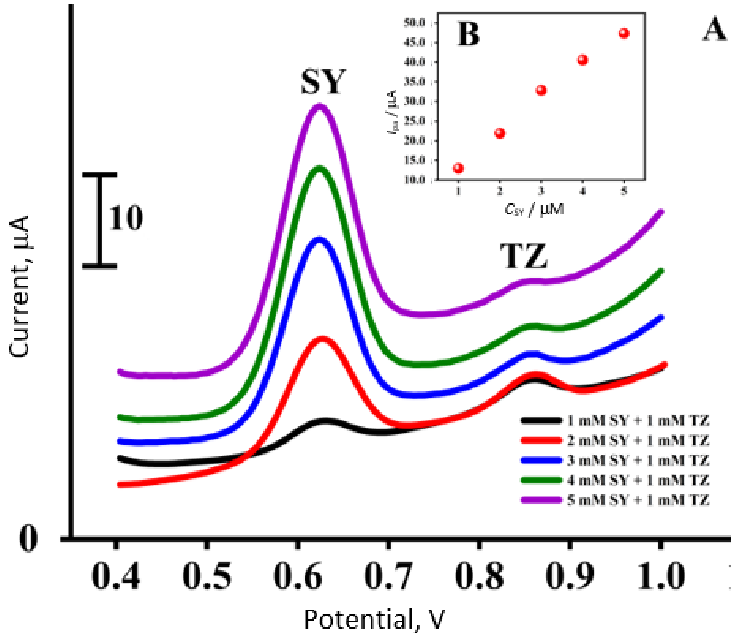

Figure 14. *DPVs of varied concentrations of SY in the presence of 1 mM TZ in 0.2 M PBS, pH 7.4; (B)* I_{pa} vs. *concentration of SY*

Similarly, Figure 15A presents the selectivity study of TZ in the presence of SY. When the concentration of TZ is increased from 1 mM to 5 mM while keeping SY concentration constant at 1 mM, the peak current of TZ also increases, while the peak current of SY remains largely unchanged with minimal fluctuations [58].

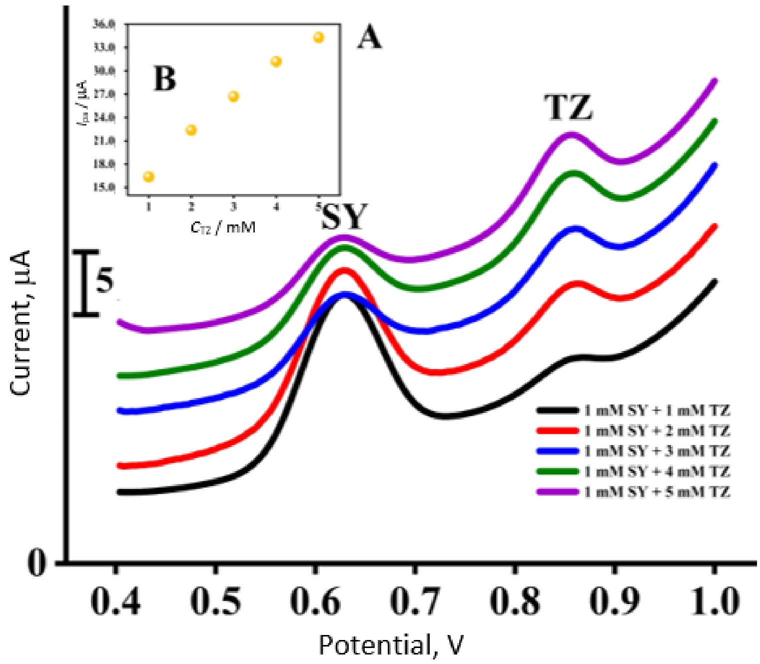

Figure 15. *(A) DPVs of varied concentrations of TZ in the presence of 1 mM SY in 0.2 M PBS, pH 7.4; (B)* I_{pa} vs. *concentration of TZ*

Figure 15B shows that the increase in TZ peak current is linear, with the regression equation given by $I_{pa} = 4.466\times10^{-6}\ C_{TZ} + 1.278\times10^{-6}$ (R^2=0.993). Overall, TX-100/MPE demonstrates excellent selectivity for distinguishing between SY and TZ in a binary mixture.

Conclusion

The TX-100 modified pencil electrode (TX-100/MPE) was fabricated using the immobilization technique with the aim of obtaining valuable sensors for sunset yellow (SY) and tartrazine (TZ) azo dyes. TX-100/MPE was electrochemically characterized by comparing its sensitivity for SY and TZ with the bare pencil electrode (BPE). The modified electrode demonstrated excellent sensitivity for both SY and TZ. The pH study for SY indicated that the process involves sharing an equal number of protons and electrons. Additionally, the analysis of the scan rate change effects revealed that the reaction for both azo dyes at the TX-100/MPE is adsorption-controlled. The modified electrode achieved impressive LOD and LOQ for both SY and TZ. The voltammetric study reveals a clear peak separation between TZ and SY in a binary mixture, and selective studies confirmed the excellent separation. The reproducibility of the TX-100/MPE in SY exhibited higher stability compared to TZ. Overall, the TX-100/MPE demonstrates exceptional sensitivity, selectivity, and reproducibility for both azo dyes. The same method can also be used for other dyes with promising results.

References

[1] P. Barciela, A. Perez-Vazquez, M. A. Prieto, Azo dyes in the food industry: Features, classification, toxicity, alternatives, and regulation, *Food and Chemical Toxicology* **178** (2023) 113935. https://doi.org/10.1016/j.fct.2023.113935

[2] L.-H. Ahlström, E. Björklund, L. Mathiasson, Optimization of an analytical procedure for the determination of banned azo dyes in leather, *Analytical and Bioanalytical Chemistry* **382** (2005) 1320-1327. https://doi.org/10.1007/s00216-005-3240-2

[3] S. Sarkar, A. Banerjee, U. Halder, R. Biswas, R. Bandopadhyay, Degradation of Synthetic Azo Dyes of Textile Industry: a Sustainable Approach Using Microbial Enzymes, *Water Conservation Science and Engineering* **2** (2017) 121-131. https://doi.org/10.1007/s41101-017-0031-5

[4] Md. N. Khan, D. K. Parmar, D. Das, Recent Applications of Azo Dyes: A Paradigm Shift from Medicinal Chemistry to Biomedical Sciences, *Mini-Reviews in Medicinal Chemistry* **21** (2021) 1071-1084. https://doi.org/10.2174/1389557520999201123210025

[5] K. Mezgebe, E. Mulugeta, Synthesis and pharmacological activities of azo dye derivatives incorporating heterocyclic scaffolds: a review, *RSC Advances* **12** (2022) 25932-25946. https://doi.org/10.1039/D2RA04934A

[6] M. A. Brown, S. C. De Vito, Predicting azo dye toxicity, *Critical Reviews in Environmental Science and Technology* **23** (1993) 249-324. https://doi.org/10.1080/10643389309388453

[7] C. Ramos-Souza, D. H. Bandoni, A. P. A. Bragotto, V. V. De Rosso, Risk assessment of azo dyes as food additives: Revision and discussion of data gaps toward their improvement, *Comprehensive Reviews in Food Science and Food Safety* **22** (2023) 380-407. https://doi.org/10.1111/1541-4337.13072

[8] C. Keshava, S. Nicolai, S. V. Vulimiri, F.A. Cruz, N. Ghoreishi, S. Knueppel, A. Lenzner, P. Tarnow, J.T. Vanselow, B. Schulz, A. Persad, N. Baker, K.A. Thayer, A.J. Williams, R. Pirow, Application of systematic evidence mapping to identify available data on the potential human health hazards of selected market-relevant azo dyes, *Environment International* **176** (2023) 107952. https://doi.org/10.1016/j.envint.2023.107952

[9] F. Pirvu, V. Iancu, M. Niculescu, C. B. Lehr, L. F. Pascu, T. Galaon, Environmental detection of Brilliant Blue, Sunset Yellow and Tartrazine using direct injection HPLC-DAD technique, *Revista de Chimie* **71** (2020) 390-400. https://doi.org/10.37358/RC.20.6.8205

[10] L. Del Giovine, A. Piccioli Bocca, Determination of synthetic dyes in ice-cream by capillary electrophoresis, *Food Control* **14** (2003) 131-135. https://doi.org/10.1016/S0956-7135(02)00055-5

[11] M. Fuh, Determination of sulphonated azo dyes in food by ion-pair liquid chromatography with photodiode array and electrospray mass spectrometry detection, *Talanta* **56** (2002) 663-671. https://doi.org/10.1016/S0039-9140(01)00625-7

[12] F. Soponar, A. C. Moţ, C. Sârbu, Quantitative determination of some food dyes using digital processing of images obtained by thin-layer chromatography, *Journal of Chromatography A* **1188** (2008) 295-300. https://doi.org/10.1016/j.chroma.2008.02.077

[13] P. Amchova, F. Siska, J. Ruda-Kucerova, Safety of tartrazine in the food industry and potential protective factors, *Heliyon* **10** (2024) e38111. https://doi.org/10.1016/j.heliyon.2024.e38111

[14] H. Alp, D. Başkan, A. Yaşar, N. Yaylı, Ü. Ocak, M. Ocak, Simultaneous Determination of Sunset Yellow FCF, Allura Red AC, Quinoline Yellow WS, and Tartrazine in Food Samples by RP-HPLC, *Journal of Chemistry* **2018** (2018) 6486250. https://doi.org/10.1155/2018/6486250

[15] F. Feng, Y. Zhao, W. Yong, L. Sun, G. Jiang, X. Chu, Highly sensitive and accurate screening of 40 dyes in soft drinks by liquid chromatography-electrospray tandem mass spectrometry, *Journal of Chromatography B* **879** (2011) 1813-1818. https://doi.org/10.1016/j.jchromb.2011.04.014

[16] S. Suzuki, M. Shirao, M. Aizawa, H. Nakazawa, K. Sasa, H. Sasagawa, Determination of synthetic food dyes by capillary electrophoresis, *Journal of Chromatography A* **680** (1994) 541-547. https://doi.org/10.1016/0021-9673(94)85153-0

[17] J. Su, X. Su, Determination of tartrazine in sports drinks by a disposable electrochemical sensor modified with Co_2O_3, *Journal of Food Measurement and Characterization* **17** (2023) 5856-5863. https://doi.org/10.1007/s11694-023-02094-1

[18] E. Sohouli, A. H. Keihan, F. Shahdost-fard, E. Naghian, M. E. Plonska-Brzezinska, M. Rahimi-Nasrabadi, F. Ahmadi, A glassy carbon electrode modified with carbon nanoonions for electrochemical determination of fentanyl, *Materials Science and Engineering C* **110** (2020) 110684. https://doi.org/10.1016/j.msec.2020.110684

[19] M. Jaafariasl, E. Shams, M. K. Amini, Silica gel modified carbon paste electrode for electrochemical detection of insulin, *Electrochimica Acta* **56** (2011) 4390-4395. https://doi.org/10.1016/j.electacta.2010.12.052

[20] P. Prasertying, M. Yamkesorn, K. Chimsaard, N. Thepsuparungsikul, S. Chaneam, K. Kalcher, R. Chaisuksant, Modified pencil graphite electrode as a low-cost glucose sensor, *Journal of Science: Advanced Materials and Devices* **5** (2020) 330-336. https://doi.org/10.1016/j.jsamd.2020.07.004

[21] A. M. Nassar, H. Salah, N. Hashem, M. Khodari, H. F. Assaf, Electrochemical Sensor Based on CuO Nanoparticles Fabricated from Copper Wire Recycling-loaded Carbon Paste Electrode for Excellent Detection of Theophylline in Pharmaceutical Formulations, *Electrocatalysis* **13** (2022) 154-164. https://doi.org/10.1007/s12678-021-00698-z

[22] M. Kenarkob, Z. Pourghobadi, Electrochemical sensor for acetaminophen based on a glassy carbon electrode modified with ZnO/Au nanoparticles on functionalized multi-walled carbon nano-tubes, *Microchemical Journal* **146** (2019) 1019-1025. https://doi.org/10.1016/j.microc.2019.02.038

[23] A. Kannan, S. Manojkumar, S. Radhakrishnan, A Facile Fabrication of Poly-ethionine Film on Glassy Carbon Electrode for Simultaneous and Sensitive Detection of Dopamine and

Paracetamol, *Electroanalysis* **33** (2021) 1175-1184. https://doi.org/10.1002/elan.202060451
[24] G. Manasa, R. J. Mascarenhas, A. K. Satpati, O. J. D'Souza, A. Dhason, Facile preparation of poly(methylene blue) modified carbon paste electrode for the detection and quantification of catechin, *Materials Science and Engineering C* **73** (2017) 552-561. https://doi.org/10.1016/j.msec.2016.12.114
[25] M. Behpour, A. M. Attaran, M. M. Sadiany, A. Khoobi, Adsorption effect of a cationic surfactant at carbon paste electrode as a sensitive sensor for study and detection of folic acid, *Measurement* **77** (2016) 257-264. https://doi.org/10.1016/j.measurement.2015.09.009
[26] A. Kumaravel, M. Chandrasekaran, Nanosilver/surfactant modified glassy carbon electrode for the sensing of thiamethoxam, *Sensors and Actuators B* **174** (2012) 380-388. https://doi.org/10.1016/j.snb.2012.08.054
[27] V.G. Sree, J.I. Sohn, H. Im, Pre-Anodized Graphite Pencil Electrode Coated with a Poly(Thionine) Film for Simultaneous Sensing of 3-Nitrophenol and 4-Nitrophenol in Environmental Water Samples, *Sensors* **22** (2022) 1151. https://doi.org/10.3390/s22031151
[28] G. Tigari, J. G. Manjunatha, A surfactant enhanced novel pencil graphite and carbon nanotube composite paste material as an effective electrochemical sensor for determination of riboflavin, *Journal of Science: Advanced Materials and Devices* **5** (2020) 56-64. https://doi.org/10.1016/j.jsamd.2019.11.001
[29] I. Kralova, J. Sjöblom, Surfactants Used in Food Industry, *Journal of Dispersion Science and Technology* **30** (2009) 1363-1383. https://doi.org/10.1080/01932690902735561
[30] A.-C. Hellgren, P. Weissenborn, K. Holmberg, Surfactants in water-borne paints, *Progress in Organic Coating* **35** (1999) 79-87. https://doi.org/10.1016/S0300-9440(99)00013-2
[31] K. Furuse, Application of Surfactants in Pharmaceuticals, *Journal of Japan Oil Chemists' Society* **18** (1969) 530-542. https://doi.org/10.5650/jos1956.18.530
[32] J. K. S. Kumara, B .E. K. Swamy, G. K. Jayaprakash, S. C. Sharma, R. Flores-Moreno, K. Mohanty, S. A. Hariprasad, Effect of TX-100 pretreatment on carbon paste electrode for selective sensing of dopamine in presence of paracetamol, *Scientific Reports* **12** (2022) 20292. https://doi.org/10.1038/s41598-022-24387-z
[33] G. Kudur Jayaprakash, B.E.K. Swamy, N. Casillas, R. Flores-Moreno, Analytical Fukui and cyclic voltammetric studies on ferrocene modified carbon electrodes and effect of Triton X-100 by immobilization method, *Electrochimica Acta* **258** (2017) 1025-1034. https://doi.org/10.1016/j.electacta.2017.11.154
[34] K. Deng, C. Li, X. Li, H. Huang, Simultaneous detection of sunset yellow and tartrazine using the nanohybrid of gold nanorods decorated graphene oxide, *Journal of Electroanalytical Chemistry* **780** (2016) 296-302. https://doi.org/10.1016/j.jelechem.2016.09.040
[35] G. Liu, Y. Tang, D. Sun, Y. Wang, Determination of sunset yellow and tartrazine using silver and poly (L-cysteine) composite film modified glassy carbon electrode, *Indian Journal of Chemistry A* **55** (2020) 298-303. http://op.niscpr.res.in/index.php/IJCA/article/view/9497
[36] M. M. Charithra, J.G . Manjunatha, Enhanced voltammetric detection of paracetamol by using carbon nanotube modified electrode as an electrochemical sensor, *Journal of Electrochemical Science and Engineering* **10** (2019) 29-40. https://doi.org/10.5599/jese.717
[37] I. Baranowska, M. Koper, The Preliminary Studies of Electrochemical Behavior of Paracetamol and Its Metabolites on Glassy Carbon Electrode by Voltammetric Methods, *Electroanalysis* **21** (2009) 1194-1199. https://doi.org/10.1002/elan.200804536
[38] R. N. Hegde, N. P. Shetti, S. T. Nandibewoor, Electro-oxidation and determination of trazodone at multi-walled carbon nanotube-modified glassy carbon electrode, *Talanta* **79** (2009) 361-368. https://doi.org/10.1016/j.talanta.2009.03.064

[39] S. J. Malode, J. C. Abbar, N. P. Shetti, S .T. Nandibewoor, Voltammetric oxidation and determination of loop diuretic furosemide at a multi-walled carbon nanotubes paste electrode, *Electrochimica Acta* **60** (2012) 95-101. https://doi.org/10.1016/j.electacta.2011.11.011

[40] H. T. Purushothama, Y. Arthoba Nayaka, Electrochemical study of hydrochlorothiazide on electrochemically pre-treated pencil graphite electrode as a sensor, *Sensing and Biosensing Research* **16** (2017) 12-18. https://doi.org/10.1016/j.sbsr.2017.09.004

[41] N. S. Prinith, J. G. Manjunatha, Surfactant modified electrochemical sensor for determination of Anthrone - A cyclic voltammetry, *Materials Science for Energy Technologies* **2** (2019) 408-416. https://doi.org/10.1016/j.mset.2019.05.004

[42] H. T. Purushothama, Y. A. Nayaka, M. M. Vinay, P. Manjunatha, R. O. Yathisha, K. V. Basavarajappa, Pencil graphite electrode as an electrochemical sensor for the voltammetric determination of chlorpromazine, *Journal of Science: Advanced Materials and Devices* **3** (2018) 161-166. https://doi.org/10.1016/j.jsamd.2018.03.007

[43] M. Kumar, B. E. K. Swamy, S. Reddy, J. K. S. Kumara, W. Zhao, Electrochemical Determination of Hematoxylin by Pretreated ZnO Nanoflakes Modified Carbon Paste Electrode in the Absence and Presence of Eosin Y, *Journal of The Electrochemical Society* **167** (2020) 087511. https://doi.org/10.1149/1945-7111/ab91c9

[44] J.G. Manjunatha, A novel voltammetric method for the enhanced detection of the food additive tartrazine using an electrochemical sensor, *Heliyon* **4** (2018) e00986. https://doi.org/10.1016/j.heliyon.2018.e00986

[45] A. A. Cardenas-Riojas, S. L. Calderon-Zavaleta, U. Quiroz-Aguinaga, E. O. López, M. Ponce-Vargas, A.M. Baena-Moncada, Evaluation of an electrochemical sensor based on gold nanoparticles supported on carbon nanofibers for detection of tartrazine dye, *Journal of Solid State Electrochemistry* **27** (2023) 1969-1982. https://doi.org/10.1007/s10008-023-05438-5

[46] C. Raril, J. G. Manjunatha, Development of sodium dodecyl sulfate based electrochemical sensor for tartrazine determination, *Portugaliae Electrochimica Acta* **39** (2021) 59-70. http://dx.doi.org/10.4152/pea.202101059

[47] S. Tahtaisleyen, O. Gorduk, Y. Sahin, Electrochemical Determination of Tartrazine Using a Graphene/Poly(L-Phenylalanine) Modified Pencil Graphite Electrode, *Analytical Letters* **53** (2020) 1683-1703. https://doi.org/10.1080/00032719.2020.1716242

[48] G. Figueira Alves, L. Vinícius de Faria, T. Pedrosa Lisboa, C. Cunha de Souza, B. Luiz Mendes Fernandes, M. Auxiliadora Costa Matos, R. Camargo Matos, A portable and affordable paper electrochemical platform for the simultaneous detection of sunset yellow and tartrazine in food beverages and desserts, *Microchemical Journal* **181** (2022) 107799. https://doi.org/10.1016/j.microc.2022.107799

[49] T. Gan, J. Sun, S. Cao, F. Gao, Y. Zhang, Y. Yang, One-step electrochemical approach for the preparation of graphene wrapped-phosphotungstic acid hybrid and its application for simultaneous determination of sunset yellow and tartrazine, *Electrochimica Acta* **74** (2012) 151-157. https://doi.org/10.1016/j.electacta.2012.04.039

[50] L. Magerusan, F. Pogacean, M. Coros, C. Socaci, S. Pruneanu, C. Leostean, I.O. Pana, Green methodology for the preparation of chitosan/graphene nanomaterial through electrochemical exfoliation and its applicability in Sunset Yellow detection, *Electrochimica* Acta **283** (2018) 578-589. https://doi.org/10.1016/j.electacta.2018.06.203

[51] F. Pogacean, M. Coros, V. Mirel, L. Magerusan, L. Barbu-Tudoran, A. Vulpoi, R.-I. Stefan-van Staden, S. Pruneanu, Graphene-based materials produced by graphite electrochemical exfoliation in acidic solutions: Application to Sunset Yellow voltammetric detection, *Microchemical Journal* **147** (2019) 112-120. https://doi.org/10.1016/j.microc.2019.03.007

[52] W. Boumya, N. Taoufik, M. Achak, H. Bessbousse, A. Elhalil, N. Barka, Electrochemical sensors and biosensors for the determination of diclofenac in pharmaceutical, biological and water samples, *Talanta Open* **3** (2021) 100026. https://doi.org/10.1016/j.talo.2020.100026
[53] G. S. Sumanth, B. E. K. Swamy, K. Chetankumar, Facile fabrication of copper oxide modified sensor for determination of Mycophenolate mofetil in biological fluids: A cyclic voltammetric study, *Materials Chemistry and Physics* **307** (2023) 128118. https://doi.org/10.1016/j.matchemphys.2023.128118
[54] Y. T. Liu, J. Deng, X. L. Xiao, L. Ding, Y. L. Yuan, H. Li, X. T. Li, X. N. Yan, L. L. Wang, Electrochemical sensor based on a poly(para-aminobenzoic acid) film modified glassy carbon electrode for the determination of melamine in milk, *Electrochimica Acta* **56** (2011) 4595-4602. https://doi.org/10.1016/j.electacta.2011.02.08
[55] J.G. Manjunatha, A surfactant enhanced graphene paste electrode as an effective electrochemical sensor for the sensitive and simultaneous determination of catechol and resorcinol, *Chemical Data Collections* **25** (2020) 100331. https://doi.org/10.1016/j.cdc.2019.100331
[56] Y. J. Yang, W. Li, CTAB functionalized graphene oxide/multiwalled carbon nanotube composite modified electrode for the simultaneous determination of sunset yellow and tartrazine, *Russian Journal of Electrochemistry* **51** (2015) 218-226. https://doi.org/10.1134/S1023193515030118
[57] T. K. Aparna, R. Sivasubramanian, M. A. Dar, One-pot synthesis of Au-Cu_2O/rGO nanocomposite based electrochemical sensor for selective and simultaneous detection of dopamine and uric acid, *Journal of Alloys and Compounds* **741** (2018) 1130-1141. https://doi.org/10.1016/j.jallcom.2018.01.205
[58] D. Sun, Y. Zhang, F. Wang, K. Wu, J. Chen, Y. Zhou, Electrochemical sensor for simultaneous detection of ascorbic acid, uric acid and xanthine based on the surface enhancement effect of mesoporous silica, *Sensors and Actuators B* **141** (2009) 641-645. https://doi.org/10.1016/j.snb.2009.07.043